Analysis of Capillary End-Effects in Steady-state and Unsteady-state Gas-Oil Relative Permeability Experiments

Leili Moghadasi[1,*], *Nicola Bona*[1], *Dario Renna*[1], *Martin Bartosek*[1], *Luca Visconti*[1]

[1]eni S.p.A Milan, Italy

Abstract. Steady-state (SS) and unsteady-state (USS) gas-displacing-oil relative permeability measurements were conducted on the same reservoir core plug. The experiments were complemented with 4D X-Ray computed tomography to directly monitor the evolution of in situ saturation distributions and to assess how spatial phase partitioning influences the measured flow behavior. Gas injection caused a progressive reduction in oil saturation, with CT images revealing strong axial saturation gradients and significant capillary end-effects in both USS and SS tests. Despite the relatively high gas saturations achieved at the end of all experiments, both SS and USS gas relative permeability values remained low, indicating limited gas connectivity across the core. CT-derived saturation profiles extracted from 3D saturation maps acquired at short time intervals showed fundamentally different expressions of capillary end-effects. As expected, the USS experiments displayed a marked increase in oil saturation near the outlet face from the onset of gas breakthrough. In contrast, the SS experiments unexpectedly exhibited a pronounced decrease in oil saturation at the outlet face during all gas–oil co-injection steps. In this paper, the observed discrepancy is examined, and several possible causes are discussed. It is well established that viscous and capillary forces control pore-scale fluid configurations, and that different flow regimes may induce hysteretic and dynamic effects in the capillary pressure saturation relationship. The co-injection of oil and gas during SS tests may locally promote imbibition, resulting in a capillary pressure curve different from the drainage curve that applies to USS tests. Moreover, in SS tests capillary back-pressure at the outlet face of the sample may play a major role than in USS tests. Finally, also dynamic capillary pressure might have played a role. The combined SS, USS, and CT results highlight that capillary end-effects and phase connectivity exert strong control over gas transport during gas–oil drainage. The findings underscore the importance of acquiring spatially resolved saturation measurements over time during both SS and USS experiments to correctly interpret displacement behavior and relative permeability data.

1 Introduction

Understanding multiphase flow in porous media remains central to reservoir engineering, particularly in processes where gas displaces oil during secondary or tertiary recovery. The quantification of relative permeability curves is essential for predicting displacement efficiency, estimating hydrocarbon recovery, and designing gas assisted EOR strategies. However, despite decades of research, significant uncertainty persists regarding the consistency and interpretation of relative permeability data obtained from steady state (SS) and unsteady state (USS) core flooding experiments. These uncertainties are amplified in strongly capillary dominated systems, where phase trapping, capillary heterogeneity, and end-effects may compromise measured flow properties [1,2].

A recurring challenge in gas–oil relative permeability studies is the influence of capillary end-effects, which arise from the interplay of capillary pressure gradients, wettability, and local pore geometry. These effects may lead to non-uniform saturation profiles and can severely distort the interpretation of laboratory measured relative permeabilities, especially when high gas mobility contrasts and low interfacial tensions are involved [3,4]. While capillary end effects are typically associated with USS displacement tests where strong saturation gradients are expected, several studies indicate that SS measurements may also be significantly affected, despite the assumption that steady-state conditions promote equilibrium flow [5, 6,7,8,9].

The introduction of 4D X-ray computed tomography has provided unprecedented insight into in situ saturation development, enabling researchers to quantify spatial fluid distributions and directly identify the onset and evolution of capillary end-effects under dynamic and steady flow conditions [10]. CT-based core-flood monitoring has revealed that saturation gradients may persist even under nominally steady-state conditions and that analytical interpretations of SS versus USS measurements may oversimplify the complex redistribution of phases within the pore network [11,12].

Of particular relevance to gas oil systems is the fundamentally different capillary behaviour associated with drainage and imbibition. USS gas injection

* Corresponding author: leili.moghadasi@eni.com

commonly represents a drainage process, where the nonwetting gas phase invades oil filled pores. In contrast, SS tests involving simultaneous oil and gas co-injection may locally enforce imbibition-like conditions, leading to capillary hysteresis and the development of saturation paths that differ from those observed during pure drainage [13, 14]. These hysteretic effects can significantly alter phase connectivity and gas mobility, ultimately impacting the measured relative permeability curves.
Capillary backpressure is less documented in the literature, but it could play a significant role when the focus is on capillary end-effects. The classic assumption in SCAL studies is that capillary pressure at the core outlet is zero because fluids are continuous and their interfaces have negligible curvatures outside the core. However, it cannot be ruled out that part of the gas (which is strongly non-wetting) exits from the core in the form of isolated bubbles (that is, with a curved interface) and not just as a continuous stream. The capillary pressure at the outlet face could therefore be greater than zero, at least locally [15, 16].
Additionally, the potential presence of dynamic capillary pressure effects where the capillary pressure saturation relationship deviates from its static equilibrium form under conditions of rapid saturation change has been increasingly recognized [15]. In fast USS experiments, the system may not fully relax to equilibrium, producing transient capillary pressure distributions that differ from those prevailing during SS tests. Such dynamics can fundamentally alter saturation gradients, end-effects, and phase partitioning [14, 15].
The combination of these effects leads to a complex interplay that can produce contrasting saturation profiles and gas connectivity in nominally identical SS and USS measurements, even when performed on the same core samples under equivalent boundary conditions. Consequently, the reliability of gas relative permeability measurements and the broader interpretation of gas–oil displacement mechanisms must be critically reassessed considering spatially resolved saturation data.
The present work addresses these challenges by integrating SS and USS core-flood experiments with high resolution 4D CT imaging supported by core flow simulations.

2 Material and Methods

This study presents and compares the results of USS and SS gas-displacing-oil experiments conducted on a reservoir core plug at Swir conditions, under 3D tomography.

2.1. Core Sample

The experiments were performed on a core plug taken from a sandstone reservoir. Rock composition includes quartz (95 % wt), kaolinite (4%) and pyrite (1%). **Table 1** reports the base properties of the sample. Klinkenberg permeability was used as base permeability.

Table 1. Sample base properties

Length [cm]	Diameter [cm]	Porosity [%]	Klink Perm [mD]	Swirr [%]
7.95	3.78	19.5	413	15.5

2.2 Core Sample preparation

The sample was cleaned by cool Soxhlet extraction (total immersion) using toluene and methanol and then dried in a humidity oven (40% humidity). After measuring the RCA properties, it was saturated with synthetic brine and then brought to Swir condition with stabilized reservoir dead oil. Water displacement was performed first in the centrifuge and subsequently by flowing the dead oil. The sample was then subjected to aging at the reservoir temperature for 40 days. After ageing, it was flooded with decalin to remove the dead oil and subsequently with doped Soltrol 130 to replace the decalin. At the end of the entire process, the sample was weighed and subjected to X-ray CT scanning to verify its oil saturation. Prior to the two-phase tests, the core was equilibrated with brine and Soltrol, and absolute oil permeability together with Swir were determined.

2.3 Fluids

Three phases were involved in the test: synthetic brine, doped synthetic oil (Soltrol 130) and N_2 as gas phase. **Table 2** and **Table 3** report fluids properties at test condition (ambient pressure, temperature= 30°C)

Table 2. Composition and Salinity of SSW used for the experiments

KCl [g/L]	49.455
NaCl [g/L]	162.255
CaCl2*6H2O [g/L]	18.070
Salinity [g/L NaCl eq]	210.6

Table 3. Fluids Properties at 30°C.

Oil viscosity [cP]	Gas viscosity [cP]
1.657	0.018

2.4 Experimental Setup

Experiments are conducted by means of advanced core-flooding setup through X-Ray CT monitoring. **Fig. 1** presents a simple schematic of the core-flooding apparatus. The core-flooding rig comprises three different sections: pumping system, X-Ray CT scanner and effluent collection system.

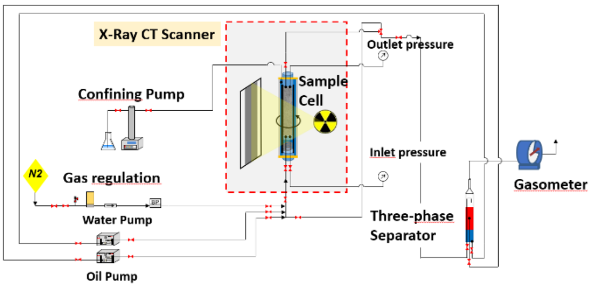

Fig. 1. Simplified schematic of the core-flooding rig used for the study

The pumping system is equipped with two syringe-type chromatographic pumps for brine and oil injection. To inject the gas phase a PC-controlled mass flow regulator is used. Downstream to the regulator, a non-return valve and a back pressure regulator are present, to avoid liquid back-flow and to maintain a stable pressure downstream to the regulator. The flow lines for fluids injection merge near the sample cell. A bypass line is used to circulate the fluid outside the sample cell, typically used to stabilize the flow, equilibrate the fluids and during the initial filling of the three-phase separator. The core sample is placed in a hassler-type core holder. A rubber sleeve surrounds laterally the core, avoiding flow between confining chamber and the rock; on top and bottom of the sample metallic heads are used to connect the sample to the flow lines. The sample is placed vertically, and fluids flow from bottom to top. The gas is injected from the bottom for reasons of greater operational ease with our experimental setup. There are two pressure transducers connected by static flow lines on inlet and outlet core head. By this method it is possible to accurately acquire differential pressure along the core therefore avoiding any error due to head-loss or line plugging. All the devices (pressure transducers, temperature sensor, gas flow) are continuously acquired by means of a proprietary data acquisition system.

2.5 Steady-State (SS) and Unsteady state (USS) relative permeability Procedure

The oil–gas relative permeability measurements were conducted under controlled steady-state flow conditions using doped Soltrol and N_2 as the two mobile phases, with the core initially at irreducible water saturation (Swi).

Steady-state measurements were performed by co-injecting Soltrol and N_2 at a constant total flow rate while imposing predefined gas fractional-flow ratios (**Table 4** and **Figure 2**). No backpressure was applied (i.e outlet pressure was the atmospheric pressure). Each flow condition was maintained until steady state was achieved, as confirmed by (i) a stable pressure differential across the core, remaining constant over at least three injected pore volumes (gas+oil) and (ii) negligible temporal variations in the saturation fields derived from computed tomography (CT). After steady-state was verified, multiple high-resolution full 3D CT scans were acquired and averaged to determine the spatial distribution of oil and gas within the core. Subsequent fractional-flow steps were imposed following a controlled two-phase drainage sequence, progressively increasing the gas injection rate while reducing the Soltrol flow rate. The CT data were processed to extract voxel-scale phase saturations, which were subsequently upscaled to obtain volume-averaged saturation values for each steady-state point.

Table 4. Oil and gas injection flow rates

Elapsed time [min]	Oil flow rate [ml/h]	Gas flow rate [ml/h]
0	240	0
10.5	180	50
1401	60	150
1764	30	181
2875	5	216
3988	0	840

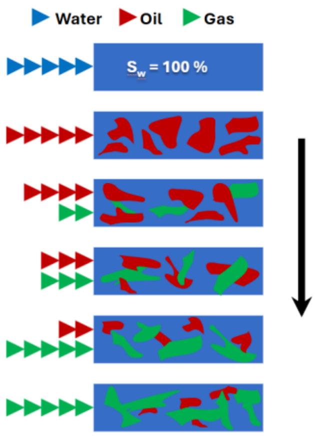

Fig. 2. SS Relative Permeability Procedure [6,7]

On completion of the steady-state (SS) protocol, the unsteady-state (USS) gas-displacement test was performed without dismounting the sample from the coreholder. The sample was brought back to oil+Swir conditions by flowing doped Soltrol 130. A backpressure of 7 bars was applied to increase gas solubility into the injected oil. After checking the oil saturation consistency and verifying that a consistent koil@Swir value was re-obtained (the initial value was 245 md and the new value was 280 md), N_2 was injected at a constant rate of 903 ml/h as a single displacing phase to mobilize oil until residual liquid saturation was reached. Like in the SS test, during the USS test the outlet pressure was atmospheric and no bump rates were performed. The USS gas injection was conducted at a gas flow rate (903 ml/h) that is comparable to the final gas flow rate of the SS test (840 ml/h). Since the magnitude of end-effects is rate-dependent, the choice not to use bumps avoided introducing an additional factor that would have complicated the end-effect analysis.

The relative permeability curves were obtained both analytically (only for the SS test) and by history matching the pressure difference across the sample versus time, the oil production curve and some 1D saturation profiles collected at different times during the experiments (both SS and USS tests). The 1D saturation profiles were derived by averaging the 3D saturation data. The history match was performed using SENDRA software [17].

2.6 CT Image Processing and Saturation Analysis

Three calibration scans were acquired: 100% oil-saturated core (CT_o), 100% gas-saturated core (CT_g) and 100% brine-saturated core (CT_w). An effective linear mixing model was applied to calculate oil and gas saturation at each voxel, i.e. $CT_{mix} = So \cdot CT_o + Sg \cdot CT_g + Sw \cdot CT_w$. Based on this relation, the irreducible water saturation (Swir) was calculated as $Swir = \frac{CT_{meas} - CT_o}{CT_w - CT_o}$, where CT_{meas} is the measured CT number at Swir conditions. Oil saturation in presence of gas + Swir was then obtained from $So = \frac{CT_{meas} - Swir \cdot CT_w - CT_g}{CT_o - CT_g}$, where CT_{meas} is the measured CT number at the new conditions. These relationships were applied on a voxel-basis for the full 3D image. From the 3D data, slice-average saturations were then calculated, for easier data interpretation and management. The saturation profiles were averaged over selected cross-sections to yield representative values of So and Sg for each fractional flow and during the USS test. Our X-ray CT system allows us to acquire the entire sample volume in approx. 2 minutes, and for these experiments we performed a full scan every 3 minutes. In the USS experiment, the gas front advanced at a linear velocity of the order 10 cm/min, so it was not possible to follow it with images. For this reason, we do not show any saturation profiles before gas breakthrough. Conversely, the saturation profiles obtained after gas breakthrough are considered sufficiently accurate, since at this stage of the USS experiment gas saturation increased more gradually and uniformly throughout the sample.

3. Results and discussion

In this section, we present the two-phase experimental results performed on the tested reservoir plug.

3.1. Steady-State test

The SS test results show consistent and physically realistic drainage relative permeability curves (**Fig. 3**). kro is 0.59 at Swir, indicating a well-connected oil phase and a relatively permeable pore system. As gas saturation increases, kro decreases smoothly and monotonically, with no irregularities and comprehensive data coverage across the saturation range. On the other hand, the krg curve remains very low up to gas saturations around 0.2, which is typical during early drainage when gas is restricted to the largest pores and oil is still strongly connected. As gas saturation increases, krg increases gradually, reaching 0.09 in the final gas-only state, which is fully consistent with expected endpoint values for a rock of this type. The visually estimated intersection of kro and krg curves is at Sg≈0.33, where both phases have approximately equal relative permeabilities (kr ≈ 0.02). This crossover point is important for reservoir simulation as it indicates the saturation at which gas and oil have similar flow capacities.

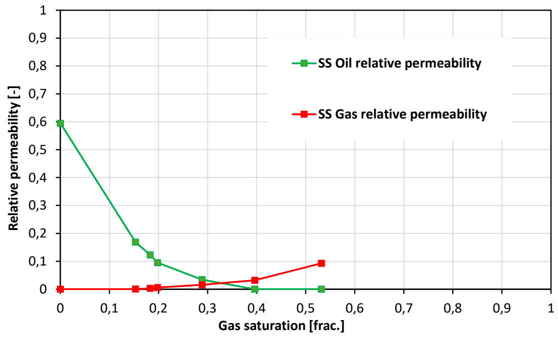

(a)

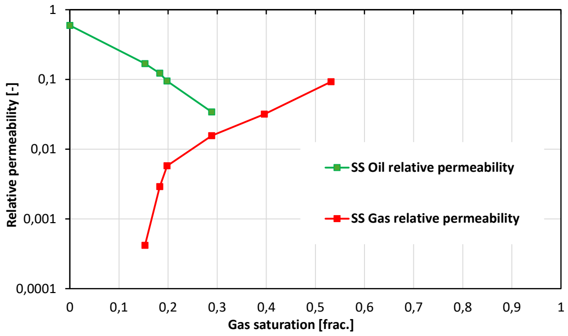

(b)

Fig. 3. Linear-scale (a) and semi-logarithmic (b) analytical relative permeability curves obtained from the steady-state experiment (Reference permeability is Klinkenberg permeability)

Overall, the data appear clean, internally consistent, and representative of high-quality steady-state measurements. **Fig. 4** shows the oil saturation profiles acquired during the experiment at the end of each injection step. They show a clear reduction of oil saturation along the core length as gas injection progresses. Oil saturation is highest near the inlet (x < 1 cm) and decreases progressively toward the outlet.

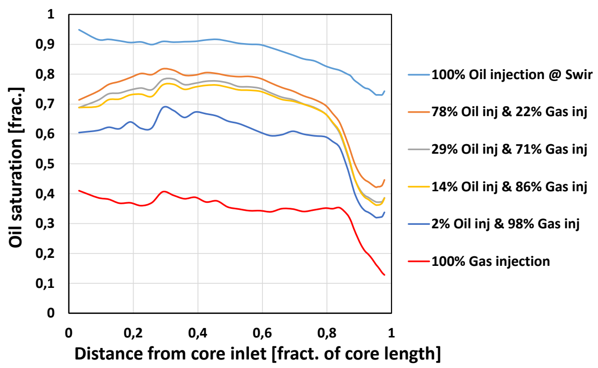

Fig. 4. In-situ saturation profiles monitored at Steady-State (SS) for the complete set of injection steps

All profiles exhibit a sharp drop in So near the outlet face (x ≈ 6–7 cm). This end-effect is anomalous because in a gas-displacing-oil experiment the distribution of fluid saturations along the core is expected to be consistent with a primary drainage Pc curve. This is positive and increases monotonically as oil saturation decreases, and so Pc is zero when oil saturation has its maximum possible value (i.e. 1-Swir). In proximity to the core outlet, therefore, where Pc gradually decreases until it becomes zero at the outlet face, oil saturation is expected to increase. Here the opposite was seen. We discuss this anomaly in a following section.

Like the 1D profiles shown in **Fig. 4**, also the 2D oil saturation maps shown in **Fig. 5** were obtained by averaging the acquired 3D saturations. The maps proceed chronologically from left to right, from single-phase oil injection at initial water saturation (Swir) to oil–gas co-injection with increasing gas fraction, and finally to single-phase gas injection at two different flow rates. Red colors correspond to high oil saturation, while green and blue indicate progressively lower oil saturation.

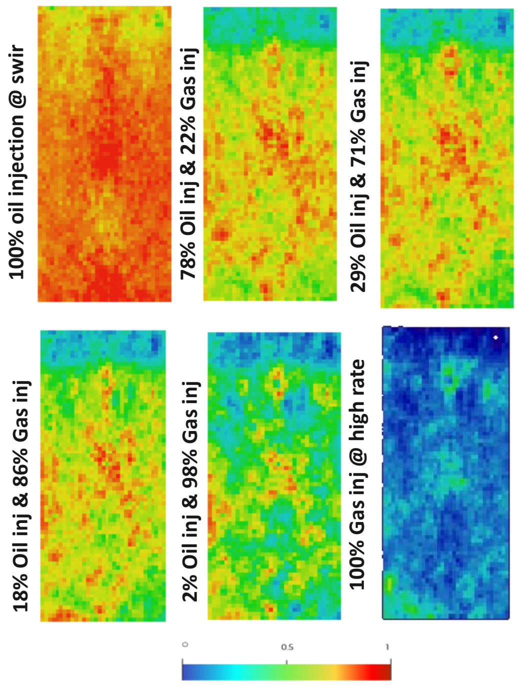

Fig. 5. X-ray CT–derived oil saturation maps during steady-state drainage under increasing gas fraction in oil–gas co-injection (Red indicates high oil saturation, while green and blue indicate progressively lower oil saturation.

At 100% oil injection, the core exhibits a relatively uniform and high oil saturation, consistent with a well-established initial Swir condition (the Sw increase towards the outlet face is attributable to rock heterogeneity). Upon introduction of gas at low fractions (15–35% gas), oil saturation decreases modestly across the core, with the reduction occurring in a spatially heterogeneous manner that reflects the underlying pore-scale structure. The anomalous end-effect, which shows a considerable oil saturation reduction in proximity to the outlet face, begins to be clearly evident already in the first injection steps. As the gas fraction increases further (65–85% gas), a more pronounced decrease in oil saturation is observed throughout the sample. Although the saturation maps exhibit small-scale heterogeneities, they appear relatively uniform at a bigger scale in the transverse direction, suggesting that gas progressively invades the pore space without forming a dominant preferential flow channel. This behavior is consistent with capillary-controlled drainage, where gas invasion occurs preferentially in larger pores while oil remains trapped in smaller pore throats. At very high gas fractions (≈98% gas) and during subsequent 100% gas injection, oil saturation is further reduced, with large portions of the core transitioning to green–blue colors. Again, residual oil remains spatially distributed and does not collapse into a single continuous low-saturation pathway.

3.2. Unsteady-State test

USS tests results are graphically illustrated in **Fig. 6-7**. Comparing USS and SS relative permeability curves (**Fig. 7**), it can be seen that the relative permeability curves obtained from the two experiments are overall similar and consistent with each other. The main differences are 1) the higher terminal gas saturation (Sgmax) value in USS and 2) a greater concavity of the krg curve in SS. Sgmax is around 0.65 in USS, while in SS it is around 0.53. Since Swir is the same, these two Sgmax values indicate a difference of 12 saturation units in the residual oil saturation Sorg. This apparent discrepancy is mainly a consequence of the fact that the USS curves shown in **Fig. 6** were obtained through history matching (Sendra software) while the SS curves of **Fig. 3** are analytical. Since Sorg was used as an unknown parameter in the USS data inversion process, it does not represent the experimental oil saturation actually obtained at the end of gas injection, but rather it should be seen as the limit value of oil saturation when an infinite volume of gas is flowed. The second difference, namely the different concavity of the krg curves with the USS curve appearing almost like a straight line, may reflect the occurrence of gas fingering mechanisms in USS, which may be partly a consequence of having injected gas from bottom. This is also supported to some extent by the krg values, which are slightly higher in USS than in SS, at equal saturation.

As anticipated, however, it is the end-effects that represent the greatest discrepancy between the two experiments and it is on these that we will focus in the discussion. The USS measurement shows the usual behavior, with oil saturation increasing towards the outlet face of the core. Here, the capillary pressure is minimal, and since the Pc curve describing the test is a gas-oil drainage curve, oil saturation at the outlet face is expected to be close to 1-Swir (i.e., around 0.7). In reality, the observed value is slightly lower than 1-Swirr (namely, around 0.6), but the fact that it remains almost constant throughout the experiment (varying between 0.55 and 0.65) is indicative of good data quality.

The oil saturation profiles are shown in **Fig. 8**, while **Fig. 9** illustrates the 2D oil saturation maps. As can be seen, oil saturation is characterized by local heterogeneities. These probably correspond to subregions of the core having contrasting porosity and permeability values. Gas (blue color) tends to slightly bypass the oil at the milli-centimetric scale (there are regions that remain yellow/green). Gas fingering might be present, as we said, However, the saturation maps do not show a well-developed gas channel, indicating that preferential gas advance should be limited to small subregions of the core.

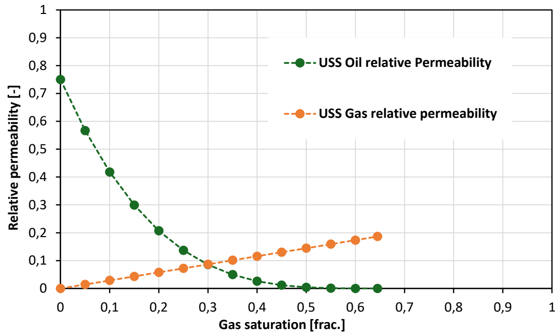

(a)

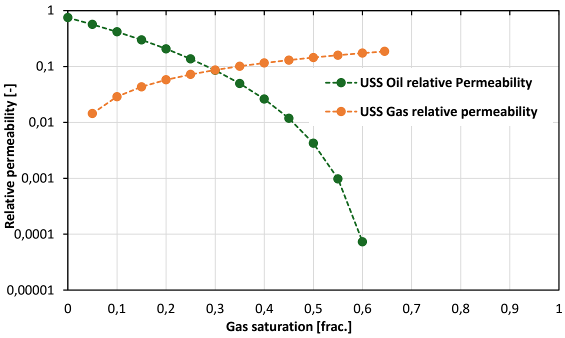

(b)

Fig. 6. Linear-scale (a) and semi-logarithmic (b) relative permeability curves obtained from the history-match (Sendra) of the Unsteady-State experiment (reference permeability is Klinkenberg permeability).

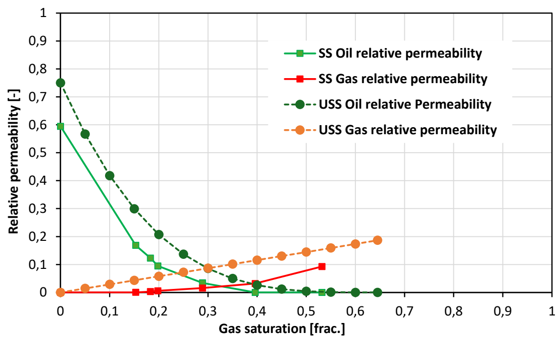

(a)

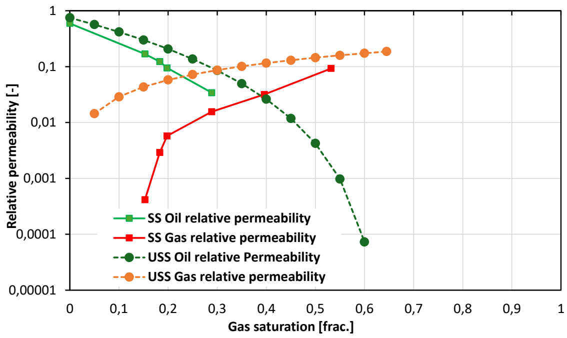

(b)

Fig. 7. Comparison of linear-scale (a) and semi-logarithmic (b) relative permeability curves shown in Fig.3 and Fig.6

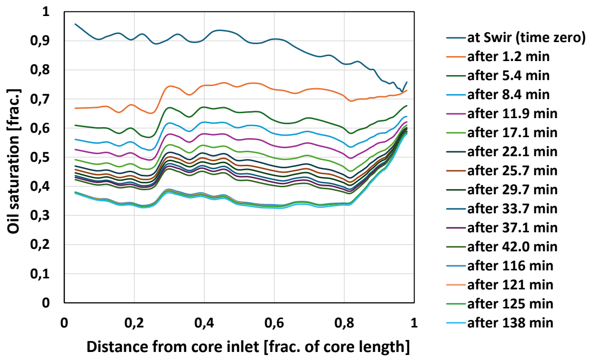

Fig. 8. In-situ saturation profiles obtained at different times during the Unsteady-State test (USS)

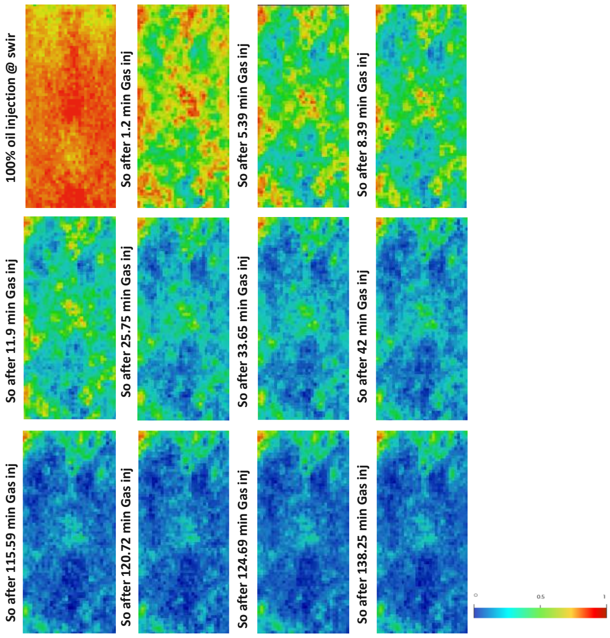

Fig.9. X-ray CT–oil saturation maps during unsteady-state drainage derived at the same times as in Fig.8 (Red indicates high oil saturation, while green and blue indicate progressively lower oil saturation.

3.3. Analysis of data

The SS and USS experiments were interpreted using Sendra software, and the results are shown in **Figs. 10-14** for the SS test and in **Figs. 15-19** for the USS test. As can be seen, the relative permeability curves obtained from the history matches are not significantly different and the Sgmax discrepancy discussed before is reconciled. In contrast, the Pc curves are very different and this is a consequence of the opposite end-effects.

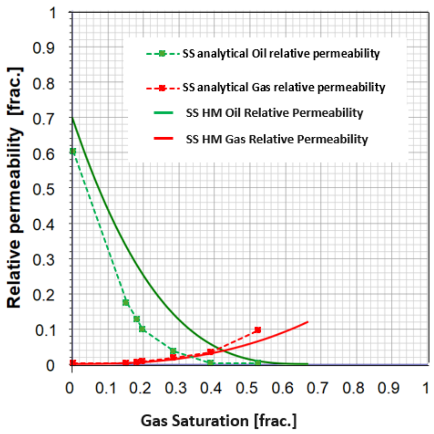

Fig. 10. Steady-State (SS) Analytical and History Match (HM)-Derived Corey Gas–Oil Relative Permeability Curves– kro(Sgi)=0.70, krg(Sorg)=0.12, Swir=0.155, Sgi=0, Sorg=0.18, No=2.85, Ng=2.60.

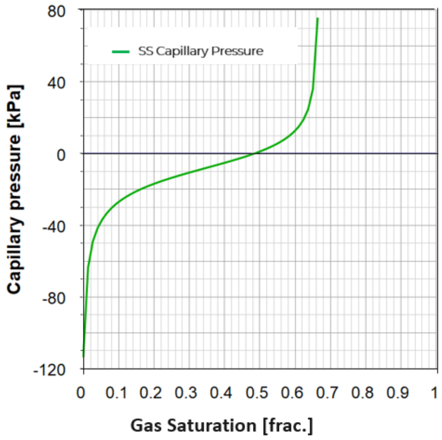

Fig. 11. SS test – Skjeveland gas-oil relative Pc curve from History Match – Co= 25 kPa, Ao=0.251, Cg=32 kPa, Ag=0.251.

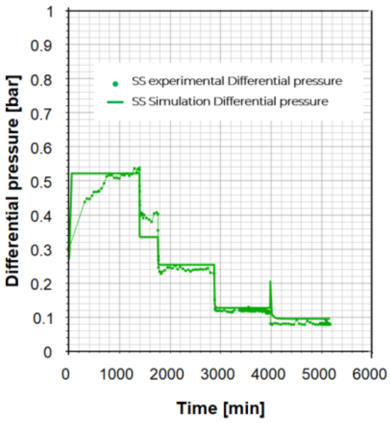

Fig. 12. SS test – History match of pressure difference across core vs time

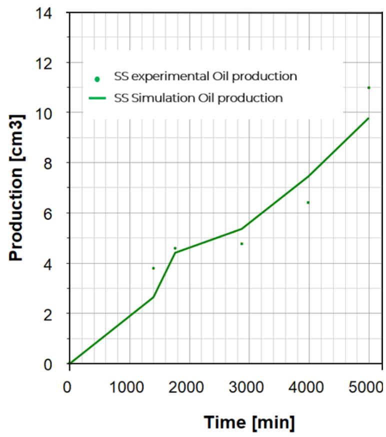

Fig. 13. SS test – History match of oil production vs time

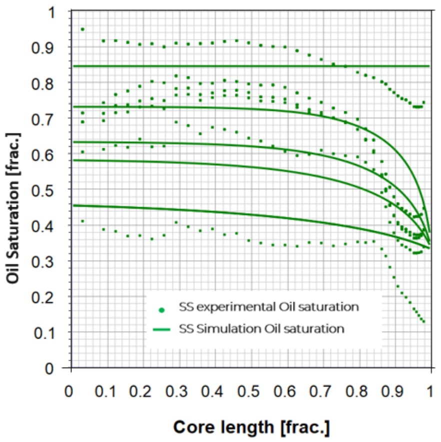

Fig. 14. SS test – History match of oil saturation profiles at end of gas-oil injection steps

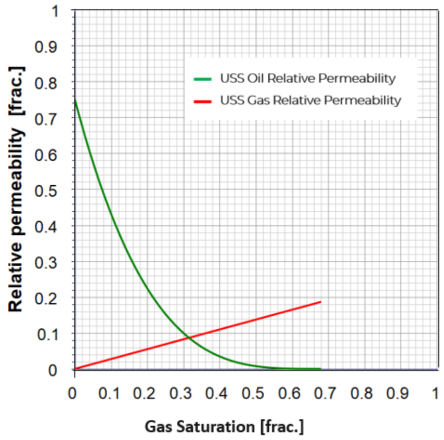

Fig. 15. USS test – Corey gas-oil relative permeability curves from History Match - referred to gas permeability – kro(Sgi)=0.75, krg(Sorg)=0.19, Swir=0.155, Sgi=0, Sorg=0.20, No=3.47, Ng=1.00.

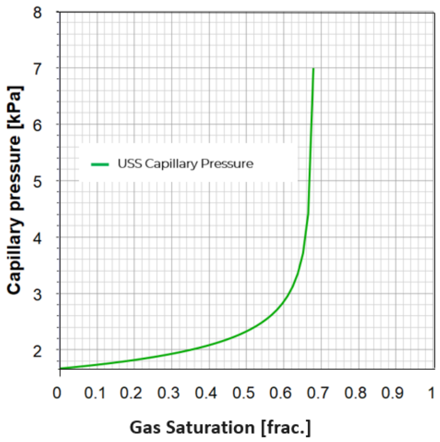

Fig. 16. USS test – Skjeveland gas-oil relative Pc curve from History Match – Co= 1.6 kPa, Ao=0.251, Cg=0

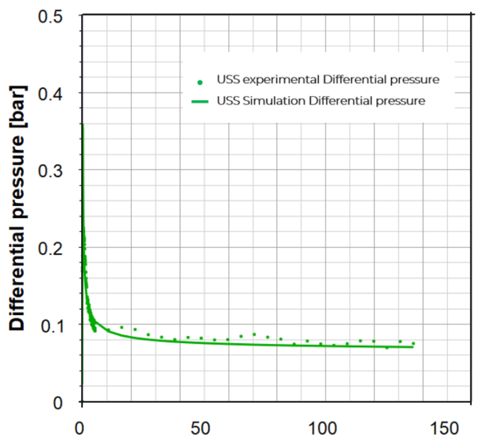

Fig. 17. USS test – History match of pressure difference across core vs time

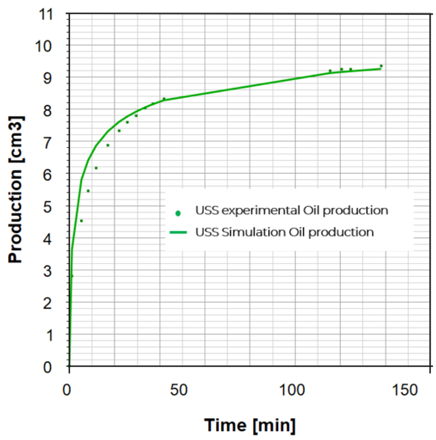

Fig. 19. USS test – History match of oil production vs time

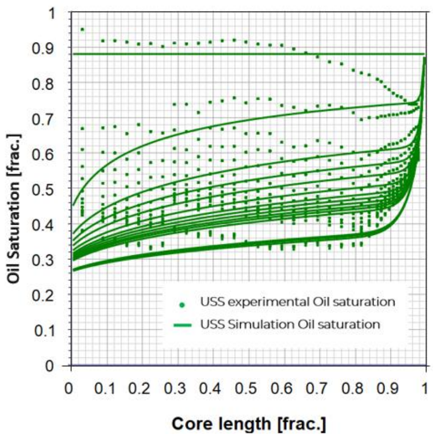

Fig. 20. USS test – History match of oil saturation profiles at end of gas-oil injection steps

4. Discussion of end-effects

While the USS test shows the expected oil saturation increase near the outlet face, which is clearly observable already from the onset of gas breakthrough, the SS experiment unexpectedly shows a marked decrease in oil saturation at the outlet face in all gas-oil co-injection steps. We exclude the occurrence of experimental problems leading to large inaccuracies in the results. It is also important to recall that the experimental setup remained the same for the two tests and the sample was not removed from the core holder between the SS and USS tests.

Three factors may have contributed to the observed end-effect discrepancy: (1) local re-imbibition, (2) capillary backpressure, and (3) dynamic capillary pressure (Pc).

4.1. Local re-imbibition

As regards local re-imbibition, co-injection of oil and gas in the SS test may have favored this type of process at the pore-scale more than single gas injection did in the USS test. Local re-imbibition occurs whenever a pore or a cluster of connected pores is first invaded by gas and then re-saturated by oil, at least partially. At the pore level, this process is not uncommon. It even occurs in primary drainage when the invading fluid withdraws from previously occupied pores to facilitate drainage of a nearby pore that has yet to be invaded [18]. Of course, if both fluids are injected, there is a larger amount of mobile oil available for re-imbibition, and it is reasonable to hypothesize that local re-imbibition processes are more likely than in single gas injection. Because of hysteresis, local re-imbibition will cause the Pc-So relationship to be different from that of a drainage (namely, lower Pc values are expected for the same saturations). These mechanisms occur at the pore scale but also the macroscopic Pc curve (which is the average of all microscopic contributions) will be affected to some extent. As a result, oil saturation in a SS test might be lower than in a USS test for the same applied capillary pressure. Near the core outlet, where drainage capillary pressure curves flatten, the difference can be notable because little variations in Pc can lead to relatively large variations in the corresponding oil saturations. This might have contributed to the lower outlet oil saturation that we observed in the SS test.

4.2. Capillary backpressure

The second factor that may have contributed to the observed end effects discrepancy is capillary backpressure. In a gas-displacing-oil SS test, particularly during the early injection steps when a large amount of oil is pumped into the core, gas might have a certain tendency to exit the core not only as a continuous stream but also in the form of small bubbles concentrated in regions where pores are large and the capillary forces opposing the gas advance are weaker (incidentally, spontaneous water-gas imbibition behaves the same way, as gas is often seen to emerge from the core at well-defined locations). These gas bubbles are surrounded by oil, at least during the early stages of the SS test, because the end-piece that is put in contact with the sample contains a large amount of oil. Therefore, a positive capillary pressure might be generated at the bubble interface: this is of the order of $2\gamma/r$, where r is the radius of the pore from which the bubble is coming out and γ is the gas-oil interfacial tension. For a pore of radius r=10 microns, the capillary backpressure is of the order of 10 kPa. This non-zero value causes the oil saturation at the outlet face of the core to be lower than the oil saturation that would exist at zero capillary pressure, which is what is expected in a USS test where the gas exits the core as a continuous stream.

4.3. Dynamic capillary pressure

Dynamic capillary pressure is the third factor we consider. It is common experience that if for some reason a rock sample is out of capillary equilibrium, the time required for saturation to re-establish equilibrium can be long. This time depends on permeability, but also on the availability of fluids. If this availability is insufficient, reaching equilibrium can take a long time regardless of permeability. An example is a sample having a non-uniform Sw distribution, which is wrapped in plastic film to prevent water evaporation: the lack of external fluid supply may cause the mobility of one or both fluids to be low and consequently the Sw in the sample becomes uniform over a long period of time (maybe days or weeks) even if permeability is high. On the other hand, if a dry core is placed in contact with an external water reservoir, the imbibition of water is a rapid process. In these examples, the rate at which fluids are redistributed in the core depends on the external availability of the fluids. For an analogous reason, in single-gas injection, since oil is not supplied to the rock, local re-equilibration of saturation can be a lengthy process. In contrast, in oil-gas co-injection, reaching equilibrium is quicker because there is higher availability of mobile oil in/from neighboring pores. Note that the availability of mobile oil will speed up the achievement of local capillary equilibria regardless of the direction of the process (whether oil saturation decreases and the oil moves from the region under consideration to nearby pores, or oil saturation increases and nearby pores must supply oil to the region under consideration). In coreflood experiments, either USS or SS, non-equilibrium may be locally formed in regions of the core where gas flow rates are high and oil displacement by gas occurs quickly. In these regions, the amount of oil initially displaced by gas can be lower than the total amount that the gas could virtually displace at the pressure at which it entered the region. As a result, oil saturation in these regions is not capillary equilibrated initially and tends to decrease thereafter in order to achieve capillary equilibrium. In a USS experiment (single gas injection) the return to capillary equilibrium may take more than the duration of the experiment, and so the Pc-So relation may never equilibrate. In contrast, since the achievement of local capillary equilibrium is faster in a SS test, the Pc-So relation will have the time to reach a capillary-equilibrated condition.

Saturation is not capillary-equilibrated if the fluid pressure difference does not coincide with the static Pc value corresponding to that saturation. Following Hassanizadeh and Gray [19], the evolution of oil saturation in a gas-oil system toward capillary equilibrium is described by $\left[p_g(t) - p_o(t)\right] - Pc^{stat}(So(t)) =$

$-\tau \frac{\partial So(t)}{\partial t}$, where t is time, $So(t)$ is the oil saturation at time t, $p_g(t)$ and $p_o(t)$ are the gas and oil pressures at time t, $Pc^{stat}(So)$ is the value of static (equilibrium) capillary pressure curve at saturation So, and τ is a coefficient ranging from 10^4 Pa·s to 10^7 Pa·s depending on the characteristics of rock and the flow regimes [19, 20, 21]. Based on this equation, since τ is non-zero, capillary equilibrium is not established instantly, but only after a time t that is sufficiently long to allow quantity $\tau \frac{\partial So}{\partial t}$ to become sufficiently small. After this time has elapsed, oil saturation will have changed by a value equal to $\Delta So = \int \frac{\partial So}{\partial t} dt$ and the difference between the pressures of the two fluids will coincide with the value of the equilibrium Pc at the equilibrium saturation. Hassanizadeh and Gray call the actual fluid pressure difference, i.e. quantity ($p_g - p_o$), the dynamic capillary pressure, Pc^{dyn}.

Based on the considerations discussed above, we hypothesize that the following events may have occured during our SS and USS experiments - in what follows, points 1), 2), and 3) apply to both experiments ; point 4-SS) applies only to the SS experiment, while point 4-USS) applies only to the USS experiment. 1) As gas invaded the core sample, displacement of oil from certain regions of the sample into nearby pores may have occurred in a short time. 2) Due to the speed of the process, the gas may not have instantly displaced all the oil that it could potentially displace according to the static Pc-So relationship. As a result, oil saturation in these regions was not capillary equilibrated. 3) To recover capillary equilibrium, oil saturation started to decrease and the kinetics of this process is described by Hassanizadeh and Gray's equation. 4-SS) In the SS test, thanks to a greater availability of mobile oil in nearby pores, oil mobility was high enough to allow oil saturation to reach capillary equilibrium in a time that was short compared to the duration of the experiment. 4-USS) Conversely, in the USS test, due to the reduced availability of mobile oil in nearby pores (which were also being flooded by single gas), the time to reach equilibrium was greater than the duration of the experiment.
In other words, we hypothesize that the τ coefficient was smaller for the SS gas-oil co-injection and larger for the USS single-gas injection. As a result, the ($p_g - p_o$) vs So relation in the USS test remained shifted upwards compared to the static ($p_g - p_o$) vs So relation which described the SS test.

Fig.20 shows the computed primary drainage dynamic Pc curve for a strongly water wet Bentheim sandstone [21]. Here the two phases are oil and water, but they can be replaced by gas and oil, respectively, without loss of meaning. As can be seen, Pc^{dyn} is greater than Pc^{stat} by an amount ranging between approx 5 kPa and 20 kPa. The difference depends on the injected rate, which is not explicitly stated in [21]. The corner points are an artifact introduced by the computation algorithm and the correct Pc^{dyn} curve must be thought of as the best fit of the curve shown in the figure.

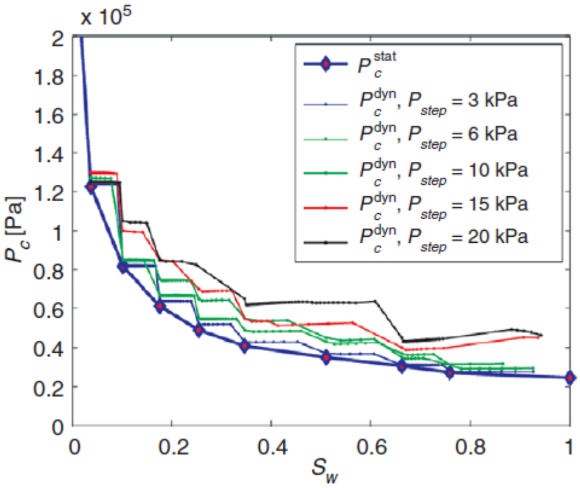

Fig. 20. Primary drainage dynamic and static capillary pressure curves computed for a Bentheim sandstone at strongly water-wet conditions [21]

Assuming that these results are representative of our experiment, we would therefore have a 5-20 kPa difference between the Pc curve associated with the SS test (which is static because in SS the local saturation perturbations had time to return to capillary equilibrium) and the curve associated with the USS test (which is dynamic because here local perturbations did not have the time to return to equilibrium). This would lead to greater oil saturation at the outlet face of the core in the USS test, as indeed has been observed.

4.4. Impact on outlet saturation

In summary, we hypothesize that in the SS experiment, there was 1) a greater occurrence of local oil re-imbibition processes, 2) possible existence of a positive capillary backpressure and 3) a Pc-So relationship that is closer to the static Pc curve. Conversely, in the USS experiment, 1) there have been fewer local re-imbibition processes, 2) the capillary pressure at the core outlet face was closer to zero and 3) the Pc-So relationship has larger So values for the same Pc because it is dynamic. All three of these factors might have caused the outlet face oil saturation in SS to be smaller than in the USS test. This would explain the observed discrepancy in the end effects, at least partially.

Let's now consider the two Pc curves obtained by history matching the experiments with SENDRA. They allow us to reproduce the observed end-effects (SS in **Fig. 11** and USS in **Fig. 16**). By shifting the SS Pc curve upward by 10 kPa (correction for backpressure effect), the intersection with the horizontal axis moves to Sg = 0.3, which means that oil saturation at the outlet face would increase by 20 saturation units.
Similarly, but in the opposite direction, by shifting the USS curve downward by 10 kPa (correction for dynamic effect), the gas saturation at which Pc=0 would increase and the corresponding oil saturation would decrease. In this case, the Pc curve would even become entirely negative, which is physically unreasonable for a single-

gas injection. This indicates that a 10 kPa correction for dynamic effects is too strong, but nonetheless the “direction” of the correction is correct.
Obviously, it is impossible to make a precise correction, and we are essentially reasoning in qualitative terms. This notwithstanding, the analysis shows that local hysteresis, capillary backpressure and dynamic Pc effects can generate variations in the Pc curve that are of the same order of magnitude as the Pc itself, thus causing considerable impacts on the end-effects and the corresponding outlet saturations.

5. Conclusions

This study compares steady state (SS) and unsteady state (USS) gas–oil relative permeability experiments performed on the same core sample, integrating conventional core flood measurements with time resolved 3D X-ray CT imaging. Although the relative permeability curves obtained from SS and USS tests are generally consistent, the experiments reveal systematic and significant differences in saturation distributions and capillary end effects.

In particular, while the USS experiment exhibits the expected increase in oil saturation toward the outlet face of the core, the SS experiment shows an unexpected decrease in oil saturation near the outlet, already evident during the early stages of gas–oil co injection. CT observations demonstrate that this behavior cannot be explained solely by a different extent of fingering phenomena in the two experiments.

The observed discrepancy between SS and USS end effects is interpreted as the combined result of three mechanisms: (i) enhanced local oil re-imbibition during gas–oil co injection in SS tests, leading to capillary hysteresis; (ii) the potential presence of a positive capillary backpressure at the outlet face during SS flow conditions; and (iii) the influence of dynamic capillary pressure effects, which may have prevented the USS experiment from reaching local capillary equilibrium within the duration of the test. These processes can induce variations in the Pc–So relationship that are comparable in magnitude to the capillary pressure itself, thereby strongly affecting outlet saturations and end effects.

The results highlight that the common assumption of local capillary equilibrium may not be always valid, even at relatively low injection rates, and that interpretation based solely on relative permeability data may be misleading without spatially and temporally resolved saturation information. The combined use of SS and USS experiments with 4D saturation imaging proves essential to correctly interpret phase connectivity, gas mobility, and displacement mechanisms in gas–oil systems.

References

1. M. Honarpour, L. Koederitz, A.H. Harvey, Relative Permeability of Petroleum Reservoirs (CRC Press, 1986)
2. M.J. Blunt, Multiphase Flow in Permeable Media: A Pore-Scale Perspective (Cambridge University Press, Cambridge, 2017)
3. D.D. Huang, M.M. Honarpour, J. Pet. Sci. Eng. 19, 103 (1998)
4. P.Ø. Andersen, Y. Zhou, J. Pet. Sci. Eng. 192, 107249 (2020)
5. S.K. Masalmeh, SCA Conference Paper 2001-23 (2001)
6. L. Moghadasi, A. Guadagnini, F. Inzoli, M. Bartosek, D. Renna, J. Pet. Sci. Eng. 145, 453 (2016)
7. L. Moghadasi, F. Inzoli, A. Guadagnini, D. Renna, M. Bartosek, G. Maddinelli, Offshore Mediterranean Conference and Exhibition, Ravenna, Italy, OMC-2017-774 (2017)
8. L. Moghadasi, A. Guadagnini, F. Inzoli, M. Bartosek, J. Pet. Sci. Eng. 135, 738 (2015)
9. S. Goodarzian, K.S. Sorbie, Geoenergy Sci. Eng. 223, 211467 (2023)
10. K.R. Tekseth, D.W. Breiby, Water Resour. Res. 60, e2023WR036514 (2024)
11. T. Bultreys, W. De Boever, V. Cnudde, Earth-Sci. Rev. 155, 93 (2016)
12. R. Pini, S.M. Benson, Water Resour. Res. 49, 3516 (2013)
13. S.M. Hassanizadeh, M.A. Celia, H.K. Dahle, Vadose Zone J. 1, 38 (2002)
14. M.C. Leverett, Trans. AIME 142, 152 (1941)
15. V. Joekar-Niasar, S.M. Hassanizadeh, Crit. Rev. Environ. Sci. Technol. 42, 1895 (2012)
16. F. Nono, P. Moonen, R. Rivenq, SCA Conference Paper 2019-019 (2019)
17. PRORES AS, Sendra – SCAL Toolbox / Core Flood Simulator, https://prores.no/solution/sendra
18. R.T. Armstrong, S. Berg, Phys. Rev. E 88, 043010 (2013)
19. S.M. Hassanizadeh, W.G. Gray, Water Resour. Res. 29, 3389 (1993)
20. V. Joekar-Niasar, S.M. Hassanizadeh, H.K. Dahle, J. Fluid Mech. 655, 38 (2010)
21. Y. Zhou, J.O. Helland, E. Jettestuen, SPE J. (2013)